

# A New Perspective on the PM Vernier Machine Mechanism

Kangfu Xie, *Student Member, IEEE*, Dawei Li\*, *Member, IEEE*, Ronghai Qu, *Senior Member, IEEE*,  
Xiang Ren, *Student Member, IEEE*, and Yuan Pan  
State Key Laboratory of Advanced Electromagnetic Engineering and Technology  
School of Electrical & Electronic Engineering, Huazhong University of Science and Technology  
\*E-mail: daweil@hust.edu.cn

**Abstract**—Permanent magnet Vernier (PMV) machines have attracted more and more attention for their merits of high torque density and simple structure. And principle of electromechanical energy conversion is the most common way to investigate the PMV machine by calculating back EMF and electromagnetic torque. In this paper, a new perspective on the mechanism of PMV machines based on the Maxwell stress tensor method is presented to deepen the insight into the reason why the force on the rotor of a PMV machine is larger than that of a SPM machine. Based on the FEA method, three machines with exactly the same rotor are analyzed and compared, namely, 24-slot/20-pole SPM, 12-slot/20-pole surface PMV and 6-slot/20-pole split-tooth PMV machines. The radial and tangential flux density and force distributions along the airgap are illustrated. It is shown that the improvement of tangential flux density in the PMV machine plays a primary role in the higher torque density, which shows a promising way to improve the torque density of machines.

**Index Terms**—Maxwell stress tensor method, Permanent magnet, Torque generation, Vernier machine.

## I. INTRODUCTION

REGARDED as an appropriate alternative for direct-drive applications, permanent magnet Vernier (PMV) machines with high torque at low speed have been widely discussed recently. The high torque density of PMV machines is attributed to the so-called magnetic gear effect, while the relationship between magnetic gear and PMV machine has been examined [1]. Owing to the larger leakage flux than conventional PM machine, the power factor of PMV machine is low, and many novel topologies have been proposed to improve the power factor or the torque density further. Since the magnets are employed in both stator and rotor side when PMV machine was firstly proposed [2], the topology has been developed further [3]-[6], while the Halbach magnet array is employed particularly. Toroidal winding is adopted in the radial [7] and axial [8] field PMV machines. With the merits of shorter end turns and thus reduced copper usage, fractional slot (FS-) PMV machine is investigated in [9], and FS winding PMV machine with two-slot coil pitch is proposed. Additionally, many more discussions about dual-rotor or dual-stator [10] [11], spoke-array [12] [13] and split-tooth [14] [15] structures have been presented.

Moreover, many technical papers have been presented to reveal the nature of Vernier machine more deeply. By the utilization of airgap permeance function, the operation principle of a Vernier machine has been discussed carefully [16] [17],

especially for different tooth-pole structures [18]. An analytical method for harmonic analysis of PMV machine is proposed by solving the field equations [19]. Further, based on the energy conversion principle, general back electromotive force (EMF) equation and analytical expression of instantaneous torque have been developed from a “macroscopic” view [20], and the design methodology has been synthesized based on the parameter effect analysis [21].

In this paper, the Maxwell stress tensor (MST) method is employed to provide a deep insight into the mechanism of PMV machines from a “microscopic” view, while the airgap flux density and force analysis are performed [22] [23]. Since surface PM and PMV machines share the same mechanical structure, except the slot configuration, a 12-slot/20-pole surface PMV and 24-slot/20-pole surface-mounted PM machine with exactly the same rotor are selected to be compared and analyzed. Besides, as another typical topology, a 6-slot/20-pole split-tooth PMV machine is also analyzed. The radial and tangential component of the airgap flux density of three machines are evaluated, so are the radial and tangential force distributions along the airgap. It is shown that due to the higher tangential airgap flux density of PMV machine, higher tangential stress and thus higher torque is generated.

## II. GENERIC TORQUE ANALYSIS

Apart from the energy balance approach to calculate the electromagnetic torque as presented in most literatures, MST method is an alternative to derive the components of force from the magnetic field. As it is closer to the physical nature of torque generation, it's better to look into the force distribution along the airgap in the machine. Specifically, the local radial and tangential components of force density within the airgap can be expressed as

$$f_r = \frac{1}{2\mu_0} (B_{gr}^2 - B_{gt}^2) \quad (1)$$

$$f_t = \frac{1}{\mu_0} B_{gr} B_{gt} \quad (2)$$

where  $f_r$  is the radial component of force density (N/m<sup>2</sup>) which is related with the vibration analysis of electric machine,  $f_t$  is the tangential component of force density which contributes to the electromagnetic torque (N/m<sup>2</sup>),  $B_{gr}$  is the radial component of airgap flux density,  $B_{gt}$  is the tangential component of airgap flux density, and  $\mu_0$  is the permeability of free space. Taking the

harmonics into account, the radial and tangential component of airgap flux density can be expanded as

$$B_{gr} = \sum_{i=1}^{\infty} B_{gri} \cos(P_{ri}\theta + \alpha_{ri}) \quad (3)$$

$$B_{gt} = \sum_{j=1}^{\infty} B_{gtj} \cos(P_{tj}\theta + \alpha_{tj}) \quad (4)$$

where  $\theta$  represents the position investigated in the airgap within the range of 0 to  $2\pi$  in radians,  $P_{ri}$  and  $P_{tj}$  represent pole pairs of radial and tangential flux density,  $\alpha_{ri}$  and  $\alpha_{tj}$  are the phase angles of corresponding harmonics of radial and tangential flux density components. Further, taking all the harmonics with different pole pairs into consideration, the electromagnetic torque can be calculated as

$$\begin{aligned} T_e &= r_g \int f_i dS = r_g^2 L_{stk} \int_0^{2\pi} \frac{B_{gr} B_{gt}}{\mu_0} d\theta \\ &= \frac{r_g^2 L_{stk}}{\mu_0} \int_0^{2\pi} \sum_{i=1}^{\infty} B_{gri} \cos(P_{ri}\theta + \alpha_{ri}) \sum_{j=1}^{\infty} B_{gtj} \cos(P_{tj}\theta + \alpha_{tj}) d\theta \\ &= \sum_{i=j=1}^{\infty} \frac{\pi r_g^2 L_{stk}}{\mu_0} B_{gri} B_{gtj} \cos(\alpha_{ri} - \alpha_{tj}) \end{aligned} \quad (5)$$

As shown above, the output torque is developed with radial and tangential component of the flux density which have the same pole pairs, and the phase difference of them. It should be noted here that tangential flux density, which is basically neglected in the analysis of most electric machines, is of great significance to the torque evaluation according to the MST method. Meanwhile, there is no ‘‘pole ratio’’ existing in the expression [20] and the phase difference between radial and tangential flux density also needs careful consideration.

Furthermore, since both  $B_{gr}$  and  $B_{gt}$  are created by two sources, armature windings and magnets for a PM machine, the radial and tangential component of flux density when saturation can be neglected are expressed as

$$B_{gr} = B_{grm} + B_{gra} \quad (6)$$

$$B_{gt} = B_{gtm} + B_{gta} \quad (7)$$

where  $B_{grm}$ ,  $B_{gtm}$ ,  $B_{gra}$  and  $B_{gta}$  denote the radial and tangential flux density created by the magnets and armature windings, respectively. Substituting the flux densities (6) and (7) into (5), the electromagnetic torque can be expressed as

$$\begin{aligned} T_e &= \sum_{i=j=1}^{\infty} \frac{\pi r_g^2 L_{stk}}{\mu_0} (B_{grmi} + B_{grai})(B_{gtmj} + B_{gtaj}) \cos(\alpha_{ri} - \alpha_{tj}) \\ &= \sum_{i=j=1}^{\infty} \frac{\pi r_g^2 L_{stk}}{\mu_0} (B_{grmi} B_{gtmj} + B_{grai} B_{gtaj} \\ &\quad + B_{grmi} B_{gtaj} + B_{grai} B_{gtmj}) \cos(\alpha_{ri} - \alpha_{tj}) \end{aligned} \quad (8)$$

According to (8), the torque  $T_e$  can be divided into four parts:

$$B_{grm} B_{gtm} \quad (i)$$

$$B_{gra} B_{gta} \quad (ii)$$

$$B_{grm} B_{gta} \quad (iii)$$

$$B_{gra} B_{gtm} \quad (iv)$$

Terms (i) and (ii) produce cogging and reluctance torque which are neglected in the following analysis. Therefore, the torque

due to other two terms can be given as

$$\begin{aligned} T_e &= \sum_{i=j=1}^{\infty} \frac{\pi r_g^2 L_{stk}}{\mu_0} [B_{grmi} B_{gtaj} \cos(\alpha_{grmi} - \alpha_{gtaj}) \\ &\quad + B_{grai} B_{gtmj} \cos(\alpha_{grai} - \alpha_{gtmj})] \end{aligned} \quad (9)$$

Based on (9), electromagnetic torque can be regarded as the result of interaction between radial and tangential flux density created by magnets and armature windings respectively. It's worth noting that the MST method is suitable for the analysis of all the machines with magnetic field as the medium for energy conversion. Therefore, MST method is selected to compare PMV with conventional PM machines to reveal their mechanism of high torque density.

### III. ELECTROMAGNETIC PERFORMANCE ANALYSIS

To offer a more intuitive observation about the higher torque density of PMV machines, three machines with same rotor are analyzed. It's known that the number of winding pole pairs  $P_s$ , rotor pole pairs  $P_r$  and the stator teeth number or flux modulator number  $Z$  should satisfy that:

$$Z = P_r \pm P_s \quad (10)$$

#### A. Machine Model

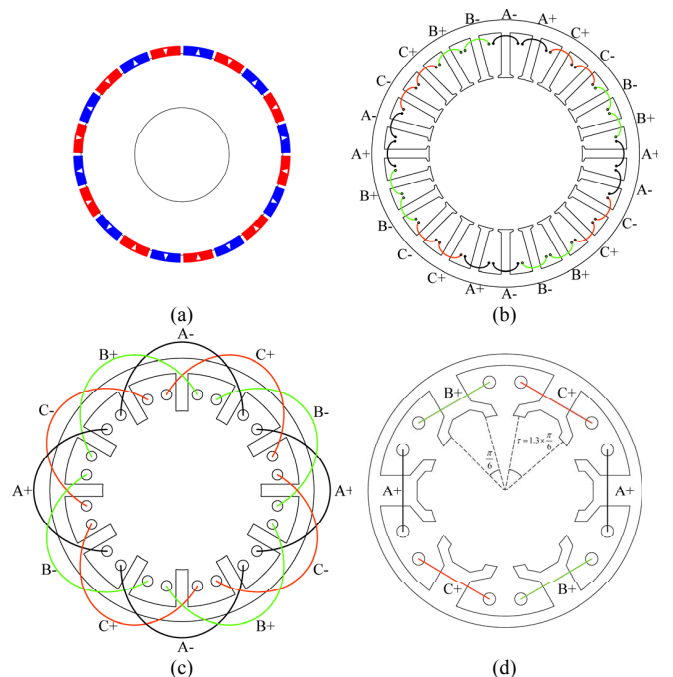


Fig. 1. Parts of the three machines. (a) The same 20-pole rotor. (b) The 24-slot stator of SPM machine. (c) The 12-slot stator of surface PMV machine. (d) The 6-slot stator of split-tooth PMV machine.

Fig. 1 shows the parts of three machines to be investigated. It should be noted that the three different machines share the same 20-pole rotor with radially magnetized magnets and the same electric loading with selected turns per slot. The material properties of magnets, stator and rotor iron, and the armature winding of the three machines are all the same. As for the 24-slot SPM machine, FSCW is employed, while the lap winding is employed in the 12-slot surface PMV machine and FSCW is employed in the 6-slot split-tooth PMV machine [15]. The

winding layouts of the three machines are also illustrated. As shown, there are auxiliary teeth working as flux modulator in the split-tooth PMV machine, and the number of auxiliary teeth, winding pole pairs and rotor pole pairs still satisfy (10). The main parameters of the three machines are given in Table I.

TABLE I  
MAIN PARAMETERS OF THE THREE MACHINES

Parameters	SPM	Surface PMV	Split-tooth PMV
Slots/Poles	24/20	12/20	6/20
NO. of flux modulators	-	-	12
Winding pole pairs	10	2	2
Winding factor	0.933	1	0.866
Outer diameter (mm)	130	124	134
Stack length (mm)	70		
Slot depth (mm)	20	17.8	14.4
Slot opening ratio	0.26	0.71	-
Turns in series per phase	200		
Airgap length (mm)	0.5		
Pole arc	0.9		
Flux modulator pitch ratio	-	-	1.3
Magnet thickness (mm)	3		

### B. Performance Comparison

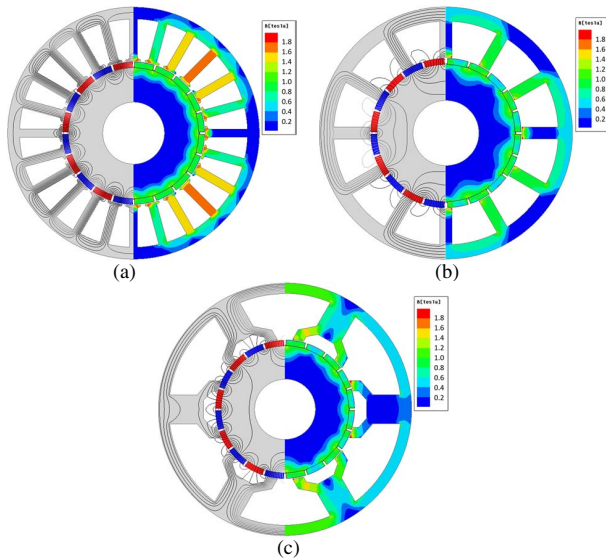


Fig. 2. Flux lines and flux density distribution under open circuit. (a) SPM machine. (b) Surface PMV machine. (c) Split-tooth PMV machine.

After the three machines were designed, the open circuit analysis and output torque under  $I_d = 0$  control are evaluated and compared by 2D FEA method, and the corresponding results are presented in Fig. 2-3. As shown in Fig. 2, it's obvious that there is 4-poles flux harmonic in both PMV machine under open circuit. Given the winding factor in Table I, it's confirmed that the PMV machine produces larger back EMF due to the more working harmonics. It's shown that the surface PMV machine and split-teeth one share the same EMF waveform, while the slot number of the two PMV machines are different and the split-teeth one features auxiliary teeth structure. The average torque of surface PMV machine is 1.5 times as that of the SPM machine owing to the magnetic gear effect, even with

the same electric loading. And the split-teeth PMV machine with merits of short end winding and lower copper loss, show 34.8% larger torque than the SPM one, while the split-teeth one get saturated easily.

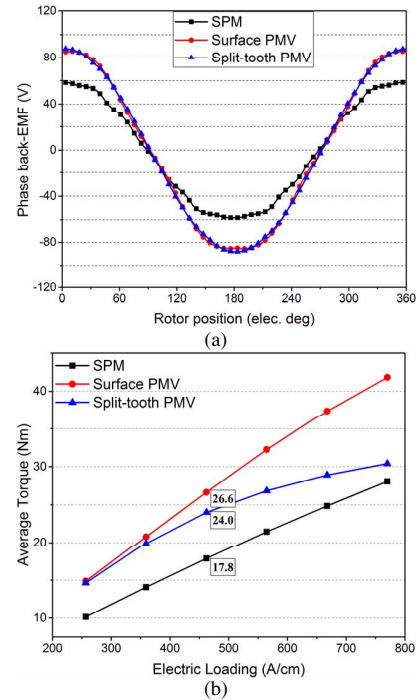


Fig. 3. Back-EMF and torque comparison of the three machines. (a) Back-EMF@600 rpm. (b) Torque vs. electric loading.

## IV. FORCE ANALYSIS

### A. Flux Density Distribution

For carefully investigation, radial and tangential flux density along the airgap of the three machines under different conditions are provided in Fig. 4.

From the waveforms under open circuit condition, it can be seen that magnets on the rotor creates a significant radial component of flux density ( $B_{grm}$ ) in the three machines, while  $B_{grm}$  of SPM machine is generally larger than that of the other two PMV machines. It's worth noting that the distortion of radial flux density waveform of PMV machines is much more serious than that of SPM machine, which makes PMV machines behave like 4 pole machines. The tangential flux density of SPM machine is almost zero, except at the positions below stator slots and magnetization direction changes. What's more interesting is that tangential flux density in PMV machines is obvious larger than that in the SPM machine, and is definitely not zero in most regions for the open slot structure. Through visual inspection, it can be seen that the multiplication of radial and tangential flux density will yield a tangential component of force density with zero average value which means no average torque for this open circuit case.

From the waveforms under load condition, compared to the open circuit, both radial and tangential flux density of the three machines in some regions are strengthened which results in higher peak values. Meanwhile, the interaction of armature reaction flux with that of the magnets results in tangential flux density with different signs from the weakened radial flux

density to produce average torque. Still, tangential flux density of PMV machines are generally larger than that of SPM one which implies the higher output torque for PMV machines.

Further, the spectra of radial and tangential airgap flux density of the three machines under different conditions are given in Fig. 5. For the SPM machine, there is main flux harmonic with 10 pole pairs which is easy to understand, while the amplitude of 14 pole pairs harmonic is quite lower, having no contribution to the average torque. For the surface PMV machine, there are flux harmonics with 10 ( $P_r$ ), 2 ( $Z - P_r$ ) and 22 ( $Z + P_r$ ) pole pairs as expected both in the radial and tangential flux density. It's quite obvious that tangential flux density of PMV machines under both open circuit and load condition is more than 2 times

as that of SPM machine, while the radial component of PMV machines is less than 80% as that of SPM machine. According to (5), it's clear that output torque of the surface PMV machine is almost 1.5 times as that of the SPM one from Fig. 5. For the split-tooth PMV machine, more flux harmonic with 4 and 16 pole pairs occur [15], due to the unequal pitch of auxiliary teeth structure. With lower winding factor and higher saturation, the output torque of split-tooth PMV machine is a little lower than that of the surface PMV machine, while the employment of FSCW makes it possible to select much higher electric loading which offsets the deficiency.

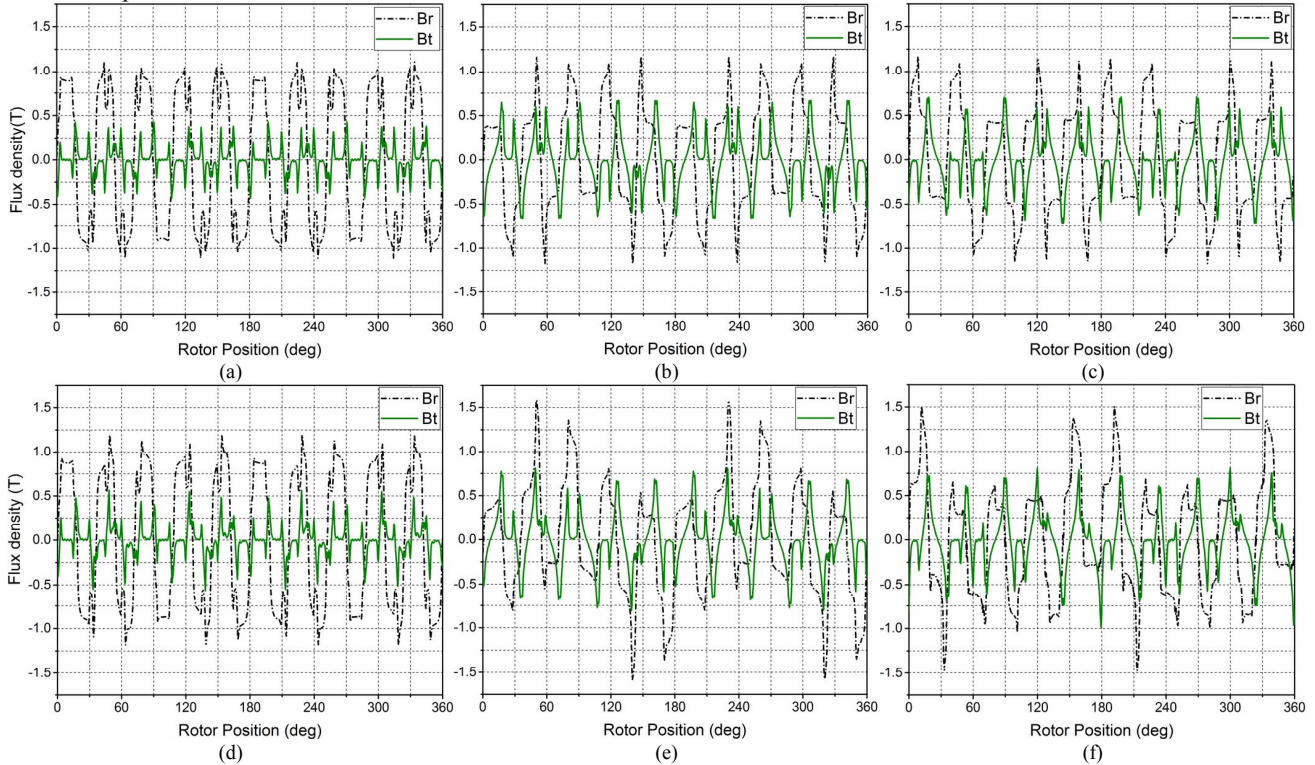


Fig. 4. Radial and tangential airgap flux density curves of the three machines. Open circuit: (a) SPM, (b) Surface PMV, (c) Split-tooth PMV. On load: (d) SPM, (e) Surface PMV, (f) Split-tooth PMV.

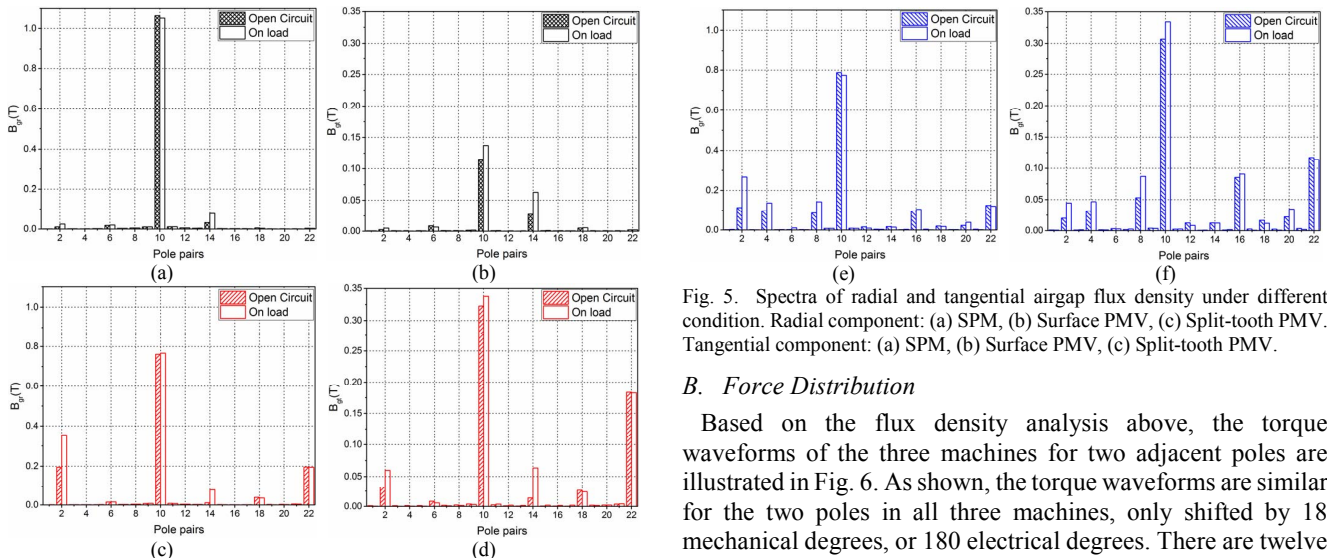


Fig. 5. Spectra of radial and tangential airgap flux density under different condition. Radial component: (a) SPM, (b) Surface PMV, (c) Split-tooth PMV. Tangential component: (a) SPM, (b) Surface PMV, (c) Split-tooth PMV.

### B. Force Distribution

Based on the flux density analysis above, the torque waveforms of the three machines for two adjacent poles are illustrated in Fig. 6. As shown, the torque waveforms are similar for the two poles in all three machines, only shifted by 18 mechanical degrees, or 180 electrical degrees. There are twelve

peaks for the SPM machine, and the period is 30 mechanical degrees, while there are six peaks for the surface PMV machine, and the corresponding period is 30 mechanical degrees, too. With unequal pitch auxiliary teeth structure employed, the period of pole torque waveform of split-tooth PMV machine is 60 mechanical degrees. Obviously, the average pole torque of PMV machines are much higher than that of the SPM one, and it's worth noting that the torque oscillation of SPM machine is lower than that of the PMV machines, while the torque ripple of them are much lower.

The dual-stator spoke-array (DSSA) PMV machine proposed in [12], is also analyzed and compared. With high torque density and high power factor, the DSSA PMV machine has two half teeth displaced stators and one rotor, while the spoke-array magnets are adopted as illustrated in Fig. 7(a). As shown in Fig. 7, the pole torque waveforms of two adjacent poles along the outer and inner airgap are calculated. Basically, the corresponding period is the same as SPM and surface PMV machine, that is, 30 mechanical degrees. What's more interesting is that the torque waveforms in the outer and inner airgap are half period shifted, and the waveform of whole pole torque is similar with SPM machine, while the average value is much higher.

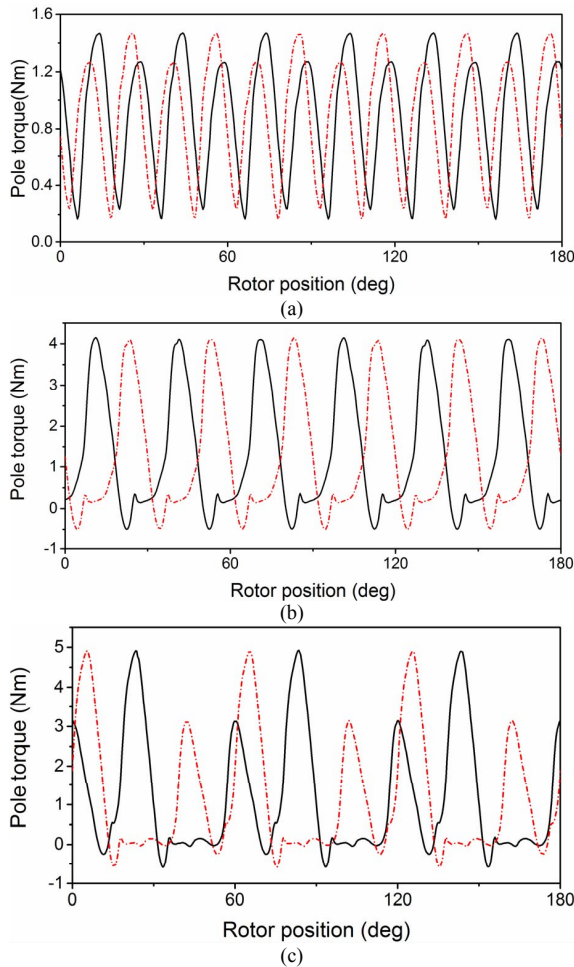


Fig. 6. Torque waveforms of two adjacent poles. (a) SPM, (b) Surface PMV, (c) Split-tooth PMV.

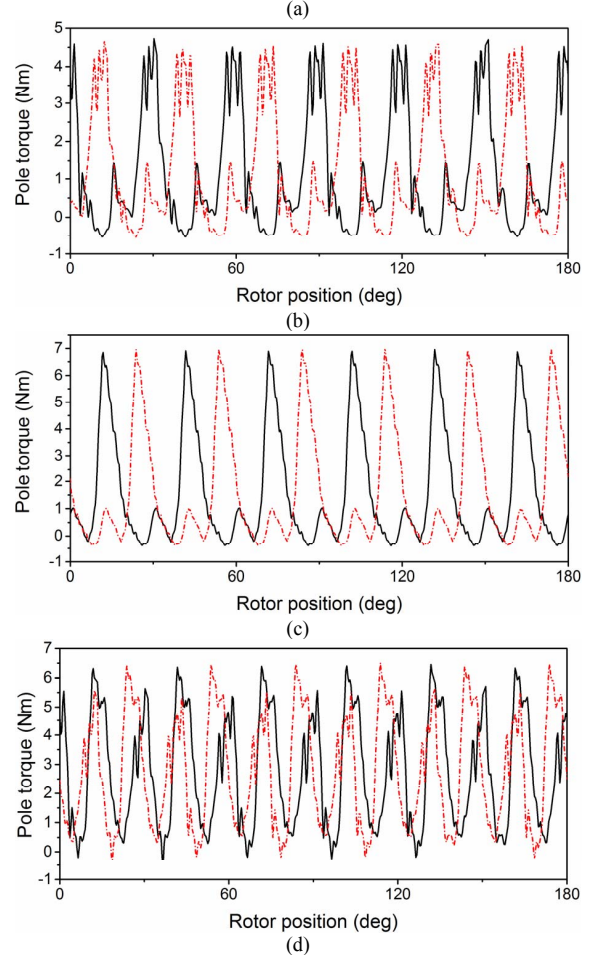
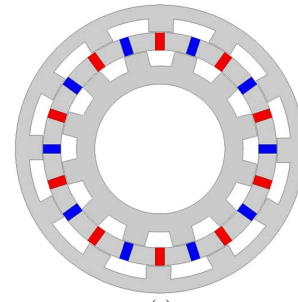


Fig. 7. Calculated torque waveforms of two adjacent poles in the DSSA PMV machine. (a) Machine model, (b) Calculated torque along the outer airgap, (c) Calculated torque along the inner airgap, (d) Calculated torque performed on the rotor.

The radial and tangential force density distributions along airgap of the three machines at selected rotor position (3.6 deg) are illustrated in Fig. 8, with the corresponding average values marked. For clarity, the negative value of tangential force is plotted so that it is not obscured by the radial force. Generally, the radial force, with no contribution to the rotation, is much larger than the tangential force in most regions for all the three machines. Specifically, the ratio of average radial force to tangential force of SPM machine is 7.7, 3.3 for the surface PMV machine, and 3 for the split-tooth PMV machine. The peak value of both radial and tangential force density of PMV machines is much higher than that of the SPM machine, while the waveforms of PMV machines are highly distorted. It's well

known and also verified here that the majority of the force (radial) produced along the airgap does not lead to rotor motion, however, a PMV machine can be taken as an example that more productive force is generated and thus the magnets are better utilized with the same rotor.

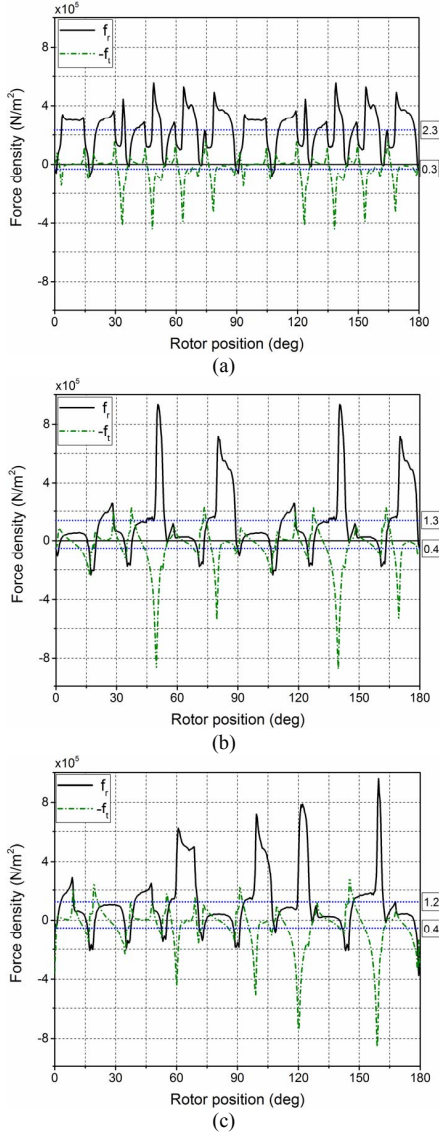


Fig. 8. Radial and tangential force density distribution of one magnet pole of the three machines. (a) SPM, (b) Surface PMV, (c) Split-tooth PMV.

### C. Calculated Torque Comparison

Referring to Fig. 5, the harmonics of flux density with significant amplitudes and their phase angle are listed in Table II. As shown below, the phase difference between  $B_{grm}$  and  $B_{gtm}$  with 10 pole pairs which are both created by magnets is technically  $90^\circ$ , so is that of  $B_{gra}$  and  $B_{gta}$ , that is to say, there is no output torque at this point. When it comes to the load condition, the phase difference changes a lot for producing the torque. It should be noted here that the phase difference of radial and tangential flux density of PMV machines under load condition is almost the same as that of the SPM one, which means that the higher tangential flux density is mainly responsible for the higher torque density of PMV machines.

With the saturation neglected, the flux density under load condition ( $B_{gr}$ ,  $B_{gt}$ ) can be calculated as the superposition of that under open circuit, namely,  $B_{gr} = B_{grm} + B_{gra}$  and  $B_{gt} = B_{gtm} + B_{gta}$ , with acceptable error. Further, the output torque is evaluated based on the flux density under load condition. It is worth noticing that flux density with 10 pole pairs has the dominant contribution to the output torque along the airgap, which is observed in all the three machines. In other words, the PMV machine can be seen as a SPM machine when seen from the rotor. When it's seen from the stator, more MMF harmonics created by excited winding are converted into the flux density with 10 pole pairs to boost the output torque. It's also important to note that  $B_{gr}$  of PMV machines is only 73% that of SPM one, and  $B_{gt}$  of PMV machines is 2.4 times as that of SPM one, while the phase angle differences are not that significant.

TABLE II  
FLUX DENSITY PARTS AND OUTPUT TORQUE

Pole pairs	$B_{grm}$ (T/deg)	$B_{gtm}$ (T/deg)	$B_{gra}$ (T/deg)	$B_{gta}$ (T/deg)	$B_{gr}$ (T/deg)	$B_{gt}$ (T/deg)	Torque (Nm)
<b>SPM</b>							
10	<b>1.06/ 90°</b>	<b>0.11/ 0°</b>	<b>0.04/ 0°</b>	<b>0.07/ 90°</b>	<b>1.05/ 85°</b>	<b>0.14/ 25°</b>	<b>17.6</b>
14	0.03/ -34°	0.03/ 145°	0.04/ 144°	0.07/ -126°	0.08/ 114°	0.06/ -156°	-
<b>17.6</b>							
<b>Surface PMV</b>							
2	0.20/ 342°	0.03/ 72°	0.30/ 72°	0.05/ 162°	0.36/ 39°	0.06/ 129°	-
10	<b>0.76/ 90°</b>	<b>0.32/ 0°</b>	<b>0.13/ 0°</b>	<b>0.09/ 90°</b>	<b>0.77/ 80°</b>	<b>0.34/ 15°</b>	<b>26.4</b>
14	0.01/ 56°	0.01/ 144°	0.08/ 144°	0.06/ -126°	0.08/ 130°	0.06/ -143°	<b>0.1</b>
22	0.20/ 162°	0.18/ -108°	0.04/ 72°	0.04/ 162°	0.20/ 147°	0.18/ -121°	<b>-0.3</b>
<b>26.2</b>							
<b>Split-tooth PMV</b>							
2	0.11/ 162°	0.02/ -108°	0.25/ 252°	0.04/ -18°	0.27/ 199°	0.04/ -42°	<b>-1.3</b>
4	0.10/ 54°	0.03/ 144°	0.11/ 324°	0.04/ 54°	0.14/ 196°	0.05/ 93°	<b>-0.4</b>
8	0.09/ 198°	0.05/ -73°	0.13/ 288°	0.08/ 18°	0.14/ 31°	0.09/ -16°	<b>2.1</b>
10	<b>0.79/ 90°</b>	<b>0.31/ 0°</b>	<b>0.13/ 0°</b>	<b>0.09/ 90°</b>	<b>0.78/ 81°</b>	<b>0.33/ 14°</b>	<b>24.0</b>
14	0.02/ 233°	0.01/ -38°	0.02/ 323°	0.02/ 54°	0.01/ 206°	0.01/ 2°	-
16	0.10/ 126°	0.09/ -144°	0.06/ 36°	0.05/ 126°	0.11/ 266°	0.09/ -171°	<b>0.5</b>
22	0.13/ 342°	0.12/ 72°	0/ 250°	0/ -18°	0.12/ 305°	0.11/ 66°	<b>-1.6</b>
<b>23.3</b>							

TABLE III  
TORQUE PARTS OF THE THREE MACHINES

	$[B_{grm}B_{gta}]$	Ratio	$[B_{gtm}B_{gra}]$	Ratio	Total
SPM	17.7	94.1%	1.1	5.9%	18.8
Surface PMV	16.3	62.2%	9.9	37.8%	26.2
Split-tooth PMV	17.0	63.9%	9.6	36.1%	26.6

As mentioned in section II, the electromagnetic torque can be divided into four parts, while only two terms, namely  $B_{grm}B_{gta}$  and  $B_{gra}B_{gtm}$  are taken into consideration, illustrated in Table III. It should be noted that only the main torque components due to 10 pole pairs flux density are compared here. Due to the local saturation in the split-tooth PMV machine, the error of

calculated torque in Table III is relatively high. Nonetheless, it's shown that the  $B_{gra}B_{gim}$  part makes a great contribution to the torque enhancement of PMV machine, while the  $B_{grm}B_{gta}$  part of the three machines does not vary that much. The output torque waveforms by FEA and MST method are compared in Fig. 9, while the rotor position selected in Table II is also marked. It's obvious that the two waveforms from two calculation methods match quite well.

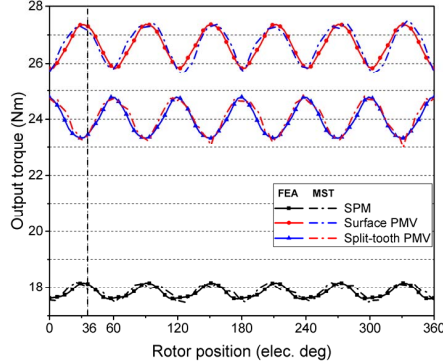


Fig. 9. Calculated torque waveforms by FEA and MST method

## V. EXPERIMENTS VALIDATION

In order to verify the analysis results, a 12-slot/20-pole PMV prototype machine is designed and tested. The main parameters are listed in Table IV. The experimental setup is shown in Fig. 10. Taking the prototype volume and heat dissipation capacity (natural cooling) into account, the winding dc copper loss including the end winding is designed as 160 W, and the electric loading is selected as 300 A/cm. The load performances of the prototype is summarized in Table V. With an electric loading of 300 A/cm and a current density of 4.75 A/mm<sup>2</sup>, the output torque of the prototype is 20.2 Nm, and the torque density is about 21 kNm/m<sup>3</sup>.

TABLE IV  
DESIGN PARAMETERS OF THE PROTOTYPE MACHINE

Parameters	Value
Slot/Pole	12/20
Outer diameter (mm)	124
Stator inner diameter (mm)	80.6
Stack length (mm)	80
Airgap length (mm)	0.8
Winding type	Single layer
Coil pitch	3
Series turns per phase	150
Pole arc	0.833
Magnet thickness (mm)	3.2
Stator tooth width (mm)	6.8
Stator yoke width (mm)	5.5
Steel lamination	35JN250
Magnet material	N38UH

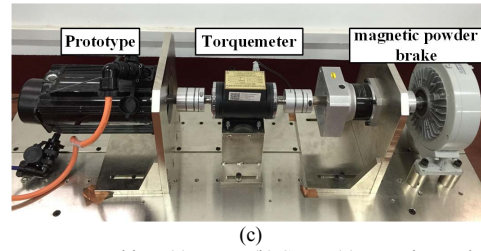
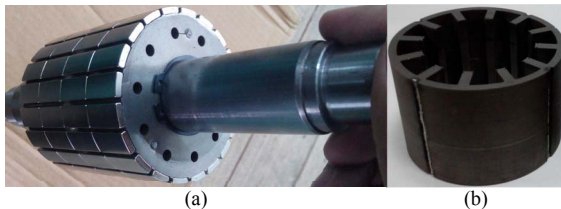


Fig. 10. Prototype machine. (a) Rotor. (b) Stator (c) Experimental setup.

TABLE V  
LOAD PERFORMANCE COMPARISON

	FEA	Measured
Speed (rpm)	500	
Current density (A/mm <sup>2</sup> )	4.75	
Electric loading (A/cm)	300	
Torque (Nm)	20.4	20.2
Efficiency	85%	84%
Power factor	0.76*	0.68

\* Neglecting the end winding inductance and resistance.

## VI. CONCLUSIONS

Three machines with the same rotor and electric loading, one SPM machine and two PMV machines, are selected to provide a new perspective on the torque producing mechanism of PMV machine. The radial and tangential component of flux density and force distribution along the airgap of 24-slot/20-pole SPM, 12-slot/20-pole surface PMV and 6-slot/20-pole split-tooth PMV machines are analyzed and compared, and the DSSA PMV machine is also analyzed to compare the torque quality. A 12-slot/20-pole PMV prototype is designed and tested to verify the FEA analysis results. It's shown that tangential flux density of PMV machines is 2.4 times as that of the SPM one which is mainly responsible for the higher torque density, while the radial flux density of PMV machine is only 73% that of the SPM one. PMV machine can be considered as a more "efficient" machine as more productive force is generated given that the majority of the force produced along the airgap does not lead to rotor motion. It's also found that magnetic field with 10 pole pairs has the dominant contribution to the output torque along the airgap. What's more important is that the omission of tangential flux density as shown in most literatures is not correct, especially for the PMV machines, and the improvement of tangential flux density offers another promising way to improve the torque density of machines further.

## ACKNOWLEDGEMENT

This work was supported by National Natural Science Foundation of China (NSFC) under Project No. 51337004 and No.51607079.

## REFERENCES

- [1] R. Qu, D. Li, and J. Wang, "Relationship between magnetic gears and vernier PM machines," in *Proc. Int. Conf. Electrical Machines & Systems*, Beijing, China, Aug. 18–20, 2011, pp:1-6.
- [2] Ishizaki, et al., "Theory and optimum design of PM vernier motor," in *Proc. IEE Int. Conf. Electrical Machines and Drives '95*, 1995, pp.208–212.

- [3] S. Niu, S. L. Ho and W. N. Fu, "A Novel Stator and Rotor Dual PM Vernier Motor With Space Vector Pulse Width Modulation," in *IEEE Trans. Magn.*, vol. 50, no. 2, pp. 805-808, Feb. 2014.
- [4] D. K. Jang and J. H. Chang, "Design of a Vernier Machine With PM on Both Sides of Rotor and Stator," in *IEEE Trans. Magn.*, vol. 50, no. 2, pp. 877-880, Feb. 2014.
- [5] W. Zhao, X. Sun, J. Ji and G. Liu, "Design and Analysis of New Vernier Permanent-Magnet Machine With Improved Torque Capability," in *IEEE Trans. Appl. Supercond.*, vol. 26, no. 4, pp. 1-5, June 2016.
- [6] K. Xie, D. Li, R. Qu and Y. Gao, "A Novel Permanent Magnet Vernier Machine With Halbach Array Magnets in Stator Slot Opening," in *IEEE Trans. Magn.*, vol. 53, no. 6, pp. 1-5, June 2017.
- [7] A. Toba and T. A. Lipo, "Novel dual-excitation permanent magnet Vernier machine," in *Conf. Rec. 34th IEEE IAS Annu. Meeting*, 1999, pp. 2539-2544.
- [8] T. Zou, R. Qu, J. Li and D. Li, "Analysis and design of a dual-rotor axial-flux vernier permanent magnet machine," in *Proc. 2015 IEEE Ener. Con. Cong. & Exp.*, pp. 3906-3913.
- [9] T. Zou, R. Qu, D. Li and D. Jiang, "Synthesis of fractional-slot vernier permanent magnet machines," *2016 XXII Int. Conf. Electr. Mac.*, pp. 911-917.
- [10] S. Niu, S. L. Ho, W. N. Fu, and L. L. Wang, "Quantitative comparison of novel Vernier permanent magnet machines," *IEEE Trans. Magn.*, vol. 46, no. 6, pp. 2032-2035, Jun. 2005.
- [11] C. Liu, K. T. Chau, J. Zhong, W. Li, and F. Li "Quantitative comparison of double-stator permanent magnet Vernier machines with and without HTS bulks," *IEEE Trans. Appl. Supercond.*, vol. 22, no. 3, Jun. 2012.
- [12] D. Li, R. Qu, and T. Lipo, "High power factor vernier permanent magnet machines," *IEEE Trans. Ind. Appl.*, vol. 50, no. 6, pp. 3664-3674, Nov./Dec. 2014.
- [13] T. Zou, D. Li, R. Qu and D. Jiang, "Performance Comparison of Surface and Spoke-Type Flux-Modulation Machines With Different Pole Ratios," in *IEEE Trans. Magn.*, vol. 53, no. 6, pp. 1-5, June 2017.
- [14] Y. Zhang, H. Lin, S. Fang, Y. Huang, H. Yang and D. Wang, "Air-Gap Flux Density Characteristics Comparison and Analysis of Permanent Magnet Vernier Machines With Different Rotor Topologies," in *IEEE Trans. Appl. Supercond.*, vol. 26, no. 4, pp. 1-5, June 2016.
- [15] T. Zou, D. Li, R. Qu, J. Li and D. Jiang, "Advanced high torque density non-overlapping winding PM vernier machines," in *Proc. 2016 IEEE Ener. Con. Cong. & Exp.*, pp. 1-8.
- [16] A. Toba and T. Lipo, "Generic torque-maximizing design methodology of surface permanent-magnet vernier machine," in *IEEE Trans. Ind. Appl.*, vol. 36, no. 6, pp. 2032-2035, Jun. 2005.
- [17] S. Taïbi, A. Tounzi, and F. Piriou, "Study of a stator current excited vernier reluctance machine," in *IEEE Trans. Energy Convers.*, vol. 21, no.4, pp. 823-831, 2006.
- [18] S. L. Ho, S. Niu and W. N. Fu, "Design and Comparison of Vernier Permanent Magnet Machines," in *IEEE Trans. Magn.*, vol. 47, no. 10, pp. 3280-3283, Oct. 2011.
- [19] J. Li, K. T. Chau and W. Li, "Harmonic Analysis and Comparison of Permanent Magnet Vernier and Magnetic-Geared Machines," in *IEEE Trans. Magn.*, vol. 47, no. 10, pp. 3649-3652, Oct. 2011.
- [20] D. Li, R. Qu, J. Li, L. Wu and W. Xu, "Analysis of torque capability and quality in vernier permanent magnet machines," in *IEEE Trans. Ind. Appl.*, vol. 52, no. 1, pp. 125-135. Jan./Feb. 2016.
- [21] L. Wu, R. Qu, D. Li and Y. Gao, "Influence of Pole Ratio and Winding Pole Numbers on Performance and Optimal Design Parameters of Surface Permanent-Magnet Vernier Machines," in *IEEE Trans. Ind. Appl.*, vol. 51, no. 5, pp. 3707-3715, Sept.-Oct. 2015.
- [22] W. Zhu, S. Pekarek, B. Fahimi and B. J. Deken, "Investigation of Force Generation in a Permanent Magnet Synchronous Machine," in *IEEE Trans. Energy Convers.*, vol. 22, no. 3, pp. 557-565, Sept. 2007.
- [23] N. Bianchi, A. Castagnini, P. S. Termini and G. Secondo, "The nature of the torque ripple in fractional-slot synchronous PMAREL machines," in *2016 IEEE Ener. Con. Cong. & Exp.*, pp. 1-8.